JMEPEG (2010) 19:541–552
DOI: 10.1007/s11665-009-9511-x

1059-9495/$19.00

Investigation of Single Pass Shape Rolling Using an Upper Bound Method

K. Abrinia and A. Fazlirad

(Submitted November 4, 2008)

This paper presents a generalized analytical upper bound method for the study of external shape, pressure, and torque in the single pass rolling of shaped sections. Generalized kinematically admissible velocity fields have been calculated from an assumed deforming geometry, in turn mathematically developed from a new parameterization of curves for the stream line flow of the material. An upper bound on rolling power was established based on the calculated velocity fields. Unknown variables in the velocity field were determined by minimizing rolling power with respect to unknown velocity field variables, yielding an upper limit to the actual power required as well as rolling pressure and torque. As an applied example, the single oval-to-round and rectangle-to-diamond roll passes have been chosen and analyzed. Velocity fields and power relations were obtained for each pass and computer analysis was carried out to analyze and simulate the process of shape rolling. External shape, average roll torque, and rolling pressure data from the analysis were compared with other worker's analytical solutions, numerical analyses, and experimental data. The results were found to be in good agreement with previous research and the method was shown to be quicker and easier to use.

Keywords oval-to-round, rectangle-to-diamond, single pass rolling, upper bound

1. Introduction

The rolling of shaped sections in industry has always been a difficult process to control and the influence of process parameters on production is of great interest. The process involves forming shapes by gradually feeding billets through grooves cut into single or multiple pairs of rolls as the billets pass through the roll gap.

To improve efficiency and product quality, designers of shape rolling processes need to optimize the amount of elongation at each pass and the geometry of roll grooves. These two parameters are dependent on the pattern of material flow through the roll cavity, stress and strain patterns on the billet, pressure distribution on the rolls, and the roll separating force. The shape of roll grooves, friction coefficient between the billet and the rolls, and the flow characteristics of the material being rolled are also significant in this regard.

Traditionally, shape rolling process design has relied on extensive experimentation and empirical formulae to develop the required parameters. In recent years, the finite element method (FEM) has been used to analyze and simulate the shape rolling process, but several drawbacks in adapting the method to shape rolling analysis still continue to prompt further research. Not only is the modeling and simulation process in FEM time consuming and difficult, it should be carried out all over again every time the shape of the rolled part is changed. Due to large deformations involved in shape rolling and the distortion of elements in FEM, convergence of the result becomes an issue which at times is impossible to deal with and at other times takes a lot of time and computer memory.

Analytical methods such as the upper bound, on the other hand, could be applied to such problems with ease and get to the results in a comparatively short time. The upper bound method used in this paper has the advantage that it is formulated in a general manner so that any process of shape rolling could be dealt with and analyzed.

With a complicated three-dimensional material flow, shape rolling analysis involves large numbers of process variables, the determination of which becomes more difficult with increasing complexity of the rolled section. As a result, empirical formulae have been developed for the design of pass sequences and the prediction of roll load and torque as well as entry and exit velocities. These formulae are limited to conventional materials and rolling conditions (Ref 1, 2).

Due to the difficulty of analytical solutions of rolling, studies have been scarce and mainly limited to specific passes. The most authoritative analytical work on rolling has been carried out by Kennedy (Ref 3). He developed an upper bound method for the analysis of metal deformation and stresses in the rolling of both flat sections and geometrical profiles without protrusions based on the general velocity fields proposed by Hill (Ref 4).

Saito et al. proposed an upper bound method that was capable of predicting lateral spread, elongation and thickness in flat, and concave (diamond) and convex (box) passes (Ref 5). Bayoumi used a flow-line field solution to analyze material flow and stresses in the steady-state rolling of the round-oval-round rolling sequence (Ref 6).

The FEM, on the other hand, has been used extensively to study both flat and shape rolling. A pioneering research work

K. Abrinia and **A. Fazlirad**, Faculty of Mechanical Engineering, College of Engineering, University of Tehran, PO Box 11155-4563, Tehran, Islamic Republic of Iran. Contact e-mail: cabrinia@ut.ac.ir.

List of Symbols

a, b	half-length of major and minor axes, respectively, of billet cross section in the oval-to-round rolling pass half-length of large and small diagonals, respectively, of exit cross section in the rectangle-to-diamond pass	V_1	velocity discontinuity at entry
		V_2	velocity discontinuity at exit
		W	total power required to deform the rolling material
		W_i	power required for plastic deformation
		W_e	power required to overcome shear forces resulting from velocity discontinuity at entry
a_1, b_1, c_1, a_2, b_2, c_2	arbitrary coefficients for the auxiliary functions of Bezier control points	W_x	power required to overcome shear forces resulting from velocity discontinuity at exit
A_1	entry cross section		
A_2	exit cross section		
A_f	roll-workpiece interface area		
f, g, h	functions of u, q, t representing position of control points in Cartesian coordinates	W_f	power required to overcome friction
		y_c	distance from the designated coordinate reference to upper roll axis
$F_0(u, q)$, $G_0(u, q)$, $H_0(u, q)$, $F_1(u, q)$, $G_1(u, q)$, $H_1(u, q)$	auxiliary functions introduced to formulate control points in Bezier curves	z_0	length of the deformation zone
		$\vec{n}$	unit vector normal to the roll surface at roll-workpiece interface
J	Jacobian for conversion of coordinates from x, y, z to u, q, t	$\vec{N}$	vector normal to the roll surface at roll-workpiece interface
m	friction shear factor	$\vec{r}(t)$	position vector of any given point on Bezier curve
P_{av}	average rolling pressure		
Q	reduction of cross-sectional area during rolling	$\vec{V}_i$	position vectors of control points on Bezier curves
r	diameter of exit cross section in the oval-to-round pass	α	angle between vector normal to the roll surface at roll-workpiece interface and the y-axis
T	roll torque		
w_0, h_0	half-length of billet sides in the rectangle-to-diamond pass	θ	angle between X or Y axes and the arbitrary end point of a streamline at exit cross section
V_x, V_y, V_z	components of the three-dimensional velocity vector	φ	angle between X or Y axes and the arbitrary start point of a streamline at entry cross section
u, q, t	parameters introduced to enable definition of deformation zone streamlines as curves		
V_e	billet velocity upon entry to the deformation zone	$\dot{\varepsilon}_{ij}$	strain rates in tensor notation
		$\bar{\dot{\varepsilon}}$	effective strain rate
V_f	velocity discontinuity at roll-workpiece interface	$\bar{\varepsilon}$	effective strain
		$\bar{\sigma}$	average flow stress
V_r	tangential roll velocity		

was carried out by Oh and Kobayashi who used the extremum principle for rigid, perfectly plastic materials in combination with numerical analysis to investigate side spread in flat rolling (Ref 7). Since then, several other researchers have used three-dimensional FEM for analyzing spread in rolling (Ref 8-10). Park and Oh developed a rigid-plastic 3D FEM code for the analysis of shape rolling processes, which is capable of handling arbitrary cross sections (Ref 10). Mori and Osakada (Ref 11, 12) developed a rigid-plastic 3D FEM to simulate steady-state deformation in shape rolling with grooved rolls. Kim et al. combined the two-dimensional rigid-plastic FEM with the slab method to reduce the amount of computation without losing accuracy (Ref 13). Hsiang and Lin developed a piecewise complex model combining the slab and FEMs. They divided the deformation zone into several slabs and used FEM to calculate sequentially the velocity field, metal flow, stress, and strain distribution for each slab (Ref 14).

Kim and Im (Ref 15) developed a three-dimensional finite element program for analyzing different shape rolling processes based on the rigid thermo-viscoplastic approach which also considered the effects of heat transfer. Deformed shape, stress, and temperature distribution in the workpiece as well as forming loads were found for square-to-oval, round-to-oval, and square-to-diamond passes and the rolling of an H-beam. Milenin et al. (Ref 16) proposed a mathematical model to address the problem of nonisothermal metal deformation during multipass rolling. The model was applied to the rolling of a steel angle bar in six passes and a double-pass round-oval-round rolling sequence.

Capece Minutolo et al. (Ref 17) used the finite element technique to analyze spread, surface profile, and cross-sectional area of the workpiece in round-to-oval and round-flat-oval passes in the rolling of steel.

Behzadipour et al. (Ref 18) introduced a neural network-based model to estimate power in flat, and shape, rolling. The model used experimental and analytical data from flat rolling for training the network and introduced a shape change quantification factor to enable application to shape rolling.

The development of an analytical, theoretically based method to predict metal flow, roll torque, rolling pressure and force, and exit velocity for shape rolling is of great benefit to the rolling industry. Such a method has been presented in

this study for the analysis of rolling of simple geometrical shapes including oval, round, rectangle, and diamond sections. The analysis assumes elastic deformations to be negligible and does not consider combined thermo-mechanical effects. A new parametric formulation has been proposed to cover the entire deformation zone, based on which strain rates and velocities are determined. The oval-to-round and diamond-to-rectangle passes have been analyzed with the new method.

2. Theory

2.1 Geometry of the Deforming Zone

The material under the action of the rolls deforms from an original shape (oval or rectangular in this paper) to a final shaped section (round and diamond, respectively). This deformation happens in a bounded region as shown for a general case in Fig. 1. It could be seen that the initial and final sections are assumed to have arbitrary shapes and considered as plane surfaces. The other surfaces of the deforming region are the roll surfaces. This geometry is now defined using curve parametric definitions.

The procedure outlined in the present study is based on the upper bound method of analysis (Ref 19). To apply the upper bound method to metal forming operations, it is first necessary to determine kinematically admissible velocity fields based on an assumption of the shape of streamlines in the deformation zone. Once the velocity fields are found, the total power dissipation for the metal forming process can be calculated. At this stage, the velocity field and power dissipation relations include unknown variables derived from the streamline formulation. As predicted power is inherently greater than the actual value required for the process, the true shape of streamlines and metal flow distribution can be found by minimizing power dissipation with respect to unknown variables of the velocity field. The minimization process will also yield an upper bound to the rolling power, from which rolling pressure and torque may be obtained.

The geometrical configuration shown for a quarter of the deformation zone in Fig. 1 is based on the choice of a streamline BB′ and a stream surface OAA′O′. The entry and exit sections are bound by planes represented by OCD and O′C′D′, respectively. To simplify relations, a left-hand coordinate system has been employed throughout this study. It has been assumed that the deformation zone consists of such stream surfaces as OAA′O′ within which streamlines such as BB′ are located. It has been further assumed that any given particle P in the deformation zone travels on such streamlines and the proportionality relation $\frac{OB}{OA} = \frac{O'B'}{O'A'}$ holds true along the entire trajectory. It can be seen that this assumption presents a method to mathematically define the deformation zone in the shape rolling of an arbitrary section to another arbitrary section (Ref 20).

To mathematically describe the streamlines, Bezier's parametric curve formulation has been employed (Ref 21). Bezier's method uses a number of control points whereby a curve of degree n has $n+1$ control points $V_i (i = 0, 1, 2, 3, \ldots n)$. The Bezier curve passes only through the first and final control points and approximates toward the intermediate points. Bezier's method also makes use of Bernstein polynomials as blending functions for the position vectors that define the control points. This research uses cubic Bezier curves.

As illustrated in Fig. 2, the curve formulated by Bezier's cubic method passes through points V_0 and V_3, and has tangents at V_0 from V_0 to V_1 and at V_3 from V_2 to V_3. It is also evident from the figure that as one or more control points are moved, the shape of the Bezier curve changes accordingly.

A typical cubic Bezier curve is defined by

$$\vec{r}(t) = (1-t)^3 \vec{V}_0 + 3t(1-t)^2 \vec{V}_1 + 3t^2(1-t)\vec{V}_2 + t^3 \vec{V}_3 \quad \text{(Eq 1)}$$

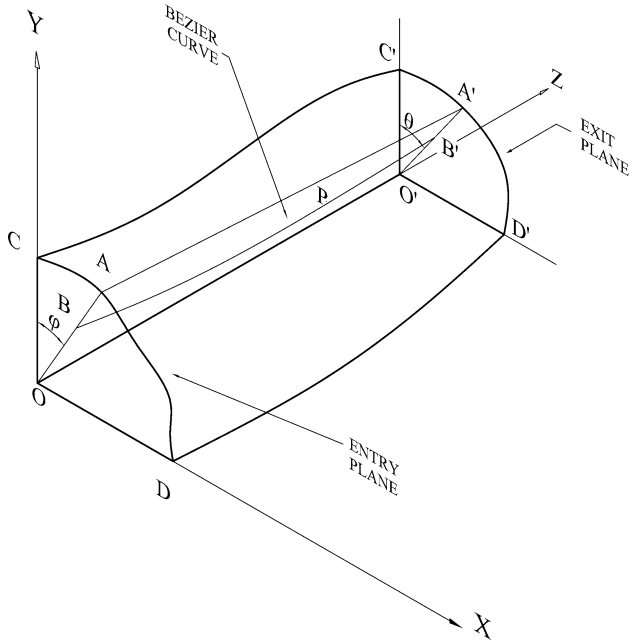

Fig. 1 A quarter of the deformation zone considered for shape rolling analysis

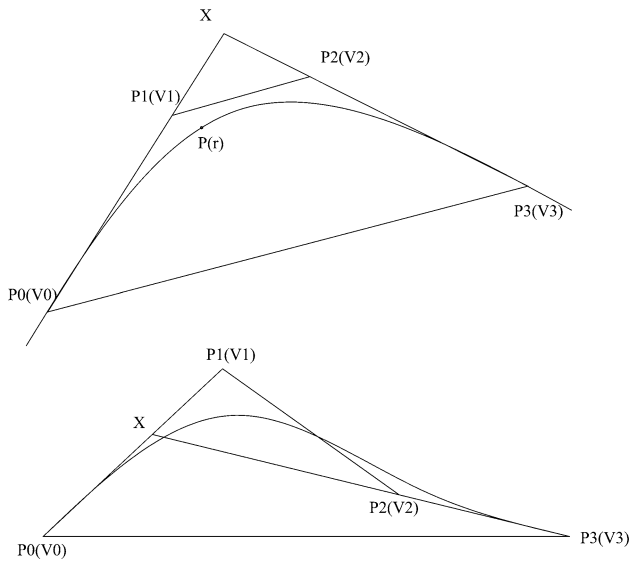

Fig. 2 A cubic Bezier curve passes through the first and last control points and approximates toward intermediate points

or in matrix notation

$$\vec{r}(t) = [\,1 \quad t \quad t^2 \quad t^3\,] \begin{bmatrix} 1 & 0 & 0 & 0 \\ -3 & 3 & 0 & 0 \\ 3 & -6 & 3 & 0 \\ -1 & 3 & -3 & 1 \end{bmatrix} \begin{bmatrix} \vec{V}_0 \\ \vec{V}_1 \\ \vec{V}_2 \\ \vec{V}_3 \end{bmatrix} \quad \text{(Eq 2)}$$

where $\vec{V}_0$ through $\vec{V}_3$ mark the position vectors of the control points, $0 \le t \le 1$ is the main curve defining parameter and $\vec{r}(t)$ is the position vector of any given point on the curve.

Expressing streamlines within the deformation zone as Bezier curves require appropriate definition of position vectors. To find relations applicable to the majority of shaped sections in industrial rolling operations, the following general format has been chosen for the vectors:

$$\begin{aligned} \vec{V}_0 &= F_0(u,q)\vec{i} + G_0(u,q)\vec{j} \\ \vec{V}_1 &= a_1F_0(u,q)\vec{i} + b_1G_0(u,q)\vec{j} + c_1H_0(u,q)\vec{k} \\ \vec{V}_2 &= a_2F_1(u,q)\vec{i} + b_2G_1(u,q)\vec{j} + c_2H_1(u,q)\vec{k} \\ \vec{V}_3 &= F_1(u,q)\vec{i} + G_1(u,q)\vec{j} + H_1(u,q)\vec{k} \end{aligned} \quad \text{(Eq 3)}$$

where u and q are two parameters that vary between 0 and 1 and control the position of vector components in the entry and exit planes. In the following sections, these parameters will be specifically defined for each rolling shape under study. F_0 and G_0 are functions of u and q that determine the location of point B (Fig. 1) and its position vector $\vec{V}_0$. In each rolling sequence subsequently studied, these functions have been defined such as to enable $\vec{V}_0$ to cover the entire entry cross section. F_1, G_1, and H_1 determine the location of point B' (Fig. 1) and position vector $\vec{V}_3$. The two intermediate control points have been defined using these same functions with H_0 added for $\vec{V}_1$ and arbitrary coefficients a_1, a_2, b_1, b_2, c_1, and c_2 introduced to adjust the position of intermediate control points.

Combining Eq 1 and 3:

$$\vec{r} = f(u,q,t)\vec{i} + g(u,q,t)\vec{j} + h(u,q,t)\vec{k} \quad \text{(Eq 4)}$$

and in the Cartesian coordinate system

$$\begin{aligned} x &= f(u,q,t) \\ y &= g(u,q,t) \\ z &= h(u,q,t) \end{aligned} \quad \text{(Eq 5)}$$

The total power W required to deform the material in a rolling operation is expressed as the sum of the following components: the power required to deform the material plastically, W_i; the power required to overcome shear forces resulting from velocity discontinuities at entry, W_e, and exit, W_x; and the power required to overcome friction, W_f. In mathematical terms

$$W = W_i + W_e + W_x + W_f \quad \text{(Eq 6)}$$

where

$$\begin{aligned} W_i &= \bar{\sigma} \int_V \left(\frac{2}{3}\dot{\varepsilon}_{ij}\dot{\varepsilon}_{ij}\right)^{1/2} dV \\ W_e &= \frac{\bar{\sigma}}{\sqrt{3}} \int_{A_1} V_1 dA_1 \\ W_x &= \frac{\bar{\sigma}}{\sqrt{3}} \int_{A_2} V_2 dA_2 \\ W_f &= \frac{m\bar{\sigma}}{\sqrt{3}} \int_{A_f} V_f dA_f \end{aligned} \quad \text{(Eq 7)}$$

Assuming the deforming material flows according to the Levy-Mises rule and obeys the Mises yield criteria (Ref 19), incompressibility—volume constancy—condition in three-dimensional metal flow can be expressed as follows:

$$\frac{\partial V_x}{\partial x} + \frac{\partial V_y}{\partial y} + \frac{\partial V_z}{\partial z} = 0 \quad \text{(Eq 8)}$$

V_x, V_y, and V_z are the components of the three-dimensional velocity vector along coordinate axes X, Y, and Z, respectively. Equating the unit tangent vector for the point P on the streamline BB' (Fig. 1) to the unit velocity vector yields:

$$\begin{aligned} V_x &= \frac{f_t}{h_t} V_z \\ V_y &= \frac{g_t}{h_t} V_z \\ V_z &= M(u,q,t) \end{aligned} \quad \text{(Eq 9)}$$

In essence, a kinematically admissible velocity field must satisfy the incompressibility condition. Replacing V_x, V_y, and V_z from (9) into (8) and solving for $M(u, q, t)$:

$$M = \frac{C \cdot h_t}{h_t(f_u g_q - f_q g_u) + h_q(f_t g_u - f_u g_t) + h_u(f_q g_t - f_t g_q)} \quad \text{(Eq 10)}$$

where C is a constant to be determined from the specific velocity boundary conditions of the section under study. Velocities calculated using (10) automatically satisfy the incompressibility condition.

Using the parametric notation employed in this study, the plastic deformation component of the total rolling power may be expressed as follows:

$$W_i = \frac{2\bar{\sigma}}{\sqrt{3}} \int_V \left(\frac{\dot{\varepsilon}_{xx}^2 + \dot{\varepsilon}_{yy}^2 + \dot{\varepsilon}_{zz}^2}{2} + \dot{\varepsilon}_{xy}^2 + \dot{\varepsilon}_{yz}^2 + \dot{\varepsilon}_{zx}^2 \right)^{1/2} |J| \cdot dudqdt \quad \text{(Eq 11)}$$

$\dot{\varepsilon}_{xx} \ldots$ are strain rates in various directions, $\bar{\sigma}$ is the flow stress and $|J|$ is the Jacobian for transformation of coordinates from x, y, z to u, q, t.

The velocity discontinuity components of total rolling power can be expressed as follows. At entry:

$$W_e = \frac{\bar{\sigma}}{\sqrt{3}} \int_0^1 \int_0^1 (V_x^2 + V_y^2)^{\frac{1}{2}} \left.\frac{\partial(x,y)}{\partial(u,q)}\right|_{t=0} dudq \quad \text{(Eq 12)}$$

At exit:

$$W_x = \frac{\bar{\sigma}}{\sqrt{3}} \int_0^1 \int_0^1 (V_x^2 + V_y^2)^{\frac{1}{2}} \left.\frac{\partial(x,y)}{\partial(u,q)}\right|_{t=1} dudq \quad \text{(Eq 13)}$$

The friction component:

$$W_f = \frac{m\bar{\sigma}}{\sqrt{3}} \int_0^1 \int_0^1 \sqrt{(V_t - V_r)^2 + V_y^2}_{u=1} \cdot \sec\alpha \cdot \left.\frac{\partial(x,z)}{\partial(q,t)}\right|_{u=1} dqdt \quad \text{(Eq 14)}$$

where $\sec\alpha = \frac{\sqrt{(N_1^2+N_2^2+N_3^2)}}{N_2}$ and $\vec{N} = \frac{\partial\vec{r}}{\partial q_{u=1}} \times \frac{\partial\vec{r}}{\partial t_{u=1}}$, $V_t = \sqrt{V_x^2 + V_z^2}$ and V_r is the tangential roll velocity.

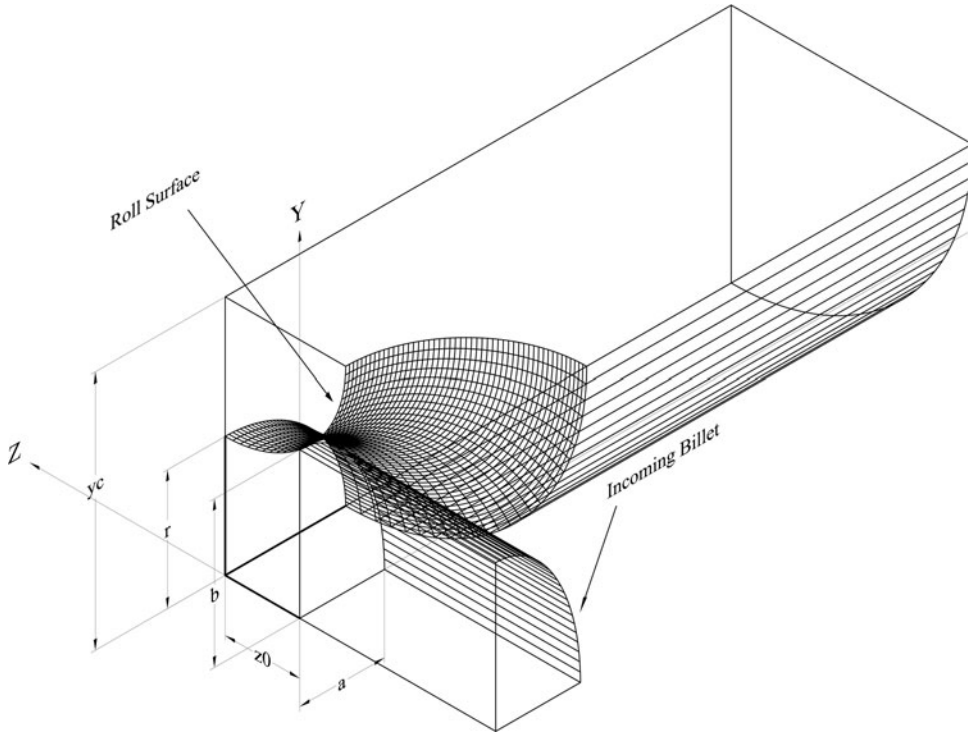

Fig. 3 A quarter of the oval-to-round pass deformation zone

3. Simulation of Pass Sequences

The analytical model presented earlier has been employed to simulate single oval-to-round and rectangle-to-diamond passes.

3.1 Oval-to-Round Pass

The oval-to-round pass is the most widely used rolling sequence for the production of round bars. Figure 3 shows a quarter of the deformation zone for the rolling of an oval billet to a round bar. Lower roll has been omitted for clarity. As the rolling geometry is assumed to be symmetrical, a quarter of the deformation zone suffices for the purpose of this analysis.

Solid grooved rolls draw the billet inside the roll gap and reduce its cross section. The projected length of the deformation zone z_0 (Fig. 3) is calculated using the geometrical particulars of the pass and billet dimensions.

This study requires an analytical representation of the three-dimensional roll groove surface. Assuming that the curve defining the exit cross section of the rolls is $y = f(x)$; every point on the roll groove surface is generated by the rotation of a corresponding point on the curve about the upper roll axis $y = y_c$. The three-dimensional roll groove surface may therefore be expressed as

$$(y_c - f(x))^2 = (y - y_c)^2 + (z_0 - z)^2 \qquad \text{(Eq 15)}$$

y and z are the coordinates of a rotated point on the roll groove surface.

The entry cross section for the oval-to-round pass is an ellipse with major and minor axes of lengths $2a$ and $2b$, respectively. The exit cross section is a circle with radius r.

The entry and exit cross sections are shown in Fig. 4.

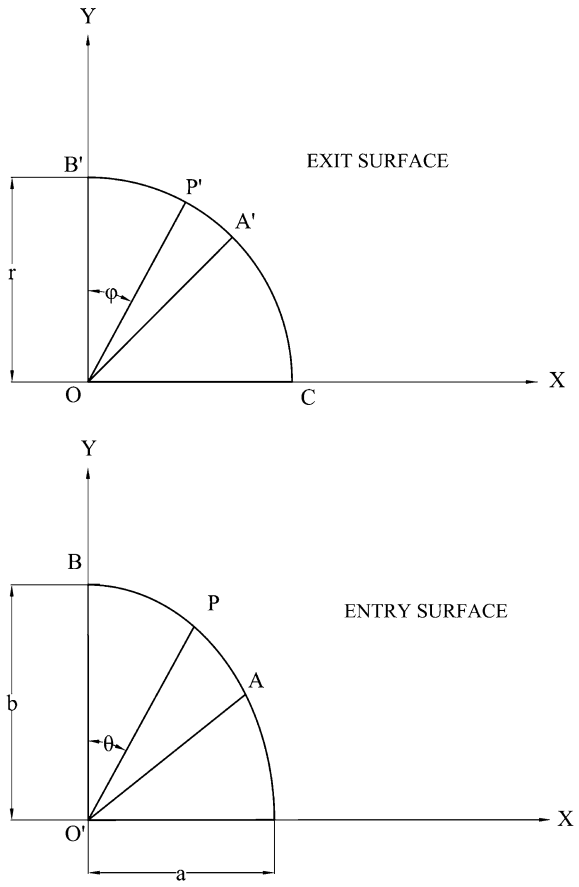

Fig. 4 Entry and exit cross sections in oval-to-round shape rolling

For the purpose of this study, a single Bezier curve was found to be sufficient to appropriately describe the entire deformation zone.

Based on Eq 3, the parametric Bezier formulation for any streamline, e.g., BB' (Fig. 1), within the deformation zone in the oval-to-round pass may be expressed as follows:

$$\begin{aligned}\vec{V}_0 &= ua\sin\varphi\cdot\vec{i} + ub\cos\varphi\cdot\vec{j}\\ \vec{V}_1 &= a_1 ua\sin\varphi\cdot\vec{i} + b_1 ub\cos\varphi\cdot\vec{j} + c_1 z_0\cdot\vec{k}\\ \vec{V}_2 &= a_2 ur\sin\varphi\cdot\vec{i} + b_2 ur\cos\varphi\cdot\vec{j} + c_2 z_0\cdot\vec{k}\\ \vec{V}_3 &= ur\sin\varphi\cdot\vec{i} + ur\cos\varphi\cdot\vec{j} + z_0\cdot\vec{k}\end{aligned} \quad \text{(Eq 16)}$$

where $\varphi = \pi q/2$ describes the angular position of the control point $\vec{V}_3$ and F_1, G_1, and H_1 in (3) have been found from the geometrical shape of the exit cross section. F_0 and G_0 in (3) have been determined from the geometry of rolling and the incompressibility condition.

The Bezier curve may be expressed in parametric terms as

$$\vec{r}(u,q,t) = (1-t)^3\vec{V}_0 + 3t(1-t^2)\vec{V}_1 + 3t^2(1-t)\vec{V}_2 + t^3\vec{V}_3 \quad \text{(Eq 17)}$$

or in Cartesian form:

$$\vec{r}(u,q,t) = f(u,q,t)\vec{i} + g(u,q,t)\vec{j} + h(u,q,t)\vec{k} \quad \text{(Eq 18)}$$

Vector $\vec{r}$ provides a parametric definition of all the streamlines in the deformation zone. Velocities in three dimensions were found to be:

$$\begin{aligned}V_z = M &= \frac{\pi V_e abu}{2\left[(f_q g_u - f_u g_q) - \frac{h_q}{h_t}(f_t g_u - f_u g_t) - \frac{h_u}{h_t}(f_q g_t - f_t g_q)\right]}\\ V_x &= \frac{f_t}{h_t}V_z\\ V_y &= \frac{g_t}{h_t}V_z\end{aligned} \quad \text{(Eq 19)}$$

where V_x, V_y, V_z represent the velocity of every point within the deformation zone in the x, y, and z coordinates, respectively, and V_e is the velocity of the oval billet at entry.

These relations satisfy both the incompressibility and velocity continuity conditions. To ensure that velocity boundary conditions are also met, a subsidiary constraint was imposed; streamlines located on the roll-workpiece interface must also be located on the roll surface. In mathematical terms, this requires that when $u = 1$, the parametric expression of the curve must satisfy the three-dimensional roll surface equation expressed in Eq 15.

The relation for power includes seven unknown coefficients; a_1 to c_2 and V_e which will be determined by the optimization of the total power required.

A MATLAB computer program utilizing the Genetic Algorithm was developed to perform the optimization. Using Simpson's three-point rule, W_i was calculated by numerical integration with respect to each of the parameters u, q, and t. For W_e and W_x, analytical integration with respect to u was followed by numerical integration with respect to q using a three-point Simpson Rule. For W_i, integration was performed numerically with respect to both parameters using Simpson's Five Point Rule.

3.2 Rectangle-to-Diamond pass

The rectangle-to-diamond pass is among the most important industrial shape rolling operations. It is both the final and intermediate pass in the production of square billets. Figure 5 shows a quarter of the deformation zone in the rolling of a rectangular billet to a diamond cross section.

It has been assumed that the entry cross section is a rectangle $2w_0$ wide and $2h_0$ high. The exit cross section is rhomboidal with a large diameter of $2a$ and a small diameter of $2b$. Unlike oval-to-round shape rolling, the deformation zone in the rectangle-to-diamond pass was found to be too complex to be appropriately described by a single Bezier curve. The deformation zone was therefore divided in two sections as shown in Fig. 6 and 7. For each section, one Bezier curve and one set of velocity field formulae were developed.

The parametric Bezier formulation for streamlines in the first half of the deformation zone may be expressed as follows:

$$\begin{aligned}\vec{V}_0 &= uh_0 tg\varphi\cdot\vec{i} + uh_0\cdot\vec{j}\\ \vec{V}_1 &= a_1 uh_0 tg\varphi\cdot\vec{i} + b_1 uh_0\cdot\vec{j} + c_1 z_0\cdot\vec{k}\\ \vec{V}_2 &= a_2 a\frac{h_0}{2w_0}\tan\varphi\cdot\vec{i} + b_2 u\frac{b(2w_0 - h_0\tan\varphi)}{2w_0}\cdot\vec{j} + c_2 z_0\cdot\vec{k}\\ \vec{V}_3 &= ua\frac{h_0}{2w_0}\tan\varphi\cdot\vec{i} + u\frac{b(2w_0 - h_0\tan\varphi)}{2w_0}\cdot\vec{j} + z_0\cdot\vec{k}\end{aligned} \quad \text{(Eq 20)}$$

where $\varphi = \pi q/4$ marks the angular position of the first control point $\vec{V}_0$. The curve itself may be expressed in parametric terms as

$$\vec{r}(u,q,t) = (1-t)^3\vec{V}_0 + 3t(1-t^2)\vec{V}_1 + 3t^2(1-t)\vec{V}_2 + t^3\vec{V}_3 \quad \text{(Eq 21)}$$

or in Cartesian form

$$\vec{r}(u,q,t) = f(u,q,t)\vec{i} + g(u,q,t)\vec{j} + h(u,q,t)\vec{k} \quad \text{(Eq 22)}$$

Velocities derived based on this curve formulation are

$$\begin{aligned}M = V_z &= \frac{\pi u V_e h_0^2}{4\cos^2\left(\frac{\pi q}{4}\right)\left[(f_q g_u - f_u g_q) - \frac{h_q}{h_t}(f_t g_u - f_u g_t) - \frac{h_u}{h_t}(f_q g_t - f_t g_q)\right]}\\ V_x &= \frac{f_t}{h_t}V_z\\ V_y &= \frac{g_t}{h_t}V_z\end{aligned} \quad \text{(Eq 23)}$$

where V_e is the velocity of the billet upon entry to the deformation zone.

The Bezier formulation for streamlines in the second half of the deformation zone has been found as

$$\begin{aligned}\vec{V}'_0 &= uw_0\cdot\vec{i} + uw_0\tan\varphi\cdot\vec{j}\\ \vec{V}'_1 &= a'_1 uw_0\cdot\vec{i} + b'_1 uw_0\tan\varphi\cdot\vec{j} + c'_1 z_0\cdot\vec{k}\\ \vec{V}'_2 &= a'_2 ua\left(\frac{2h_0 - w_0\tan\varphi}{2h_0}\right)\cdot\vec{i} + b'_2 ub\frac{w_0\tan\varphi}{2h_0}\cdot\vec{j} + c'_2 z_0\cdot\vec{k}\\ \vec{V}'_3 &= ua\left(\frac{2h_0 - w_0\tan\varphi}{2h_0}\right)\cdot\vec{i} + ub\frac{w_0\tan\varphi}{2h_0}\cdot\vec{j} + z_0\cdot\vec{k}\end{aligned} \quad \text{(Eq 24)}$$

In parametric terms and Cartesian coordinates:

$$\begin{aligned}\vec{r}'(u,q,t) &= (1-t)^3\vec{V}'_0 + 3t(1-t^2)\vec{V}'_1 + 3t^2(1-t)\vec{V}'_2 + t^3\vec{V}'_3\\ \vec{r}'(u,q,t) &= f'(u,q,t)\vec{i} + g'(u,q,t)\vec{j} + h'(u,q,t)\vec{k}\end{aligned}$$

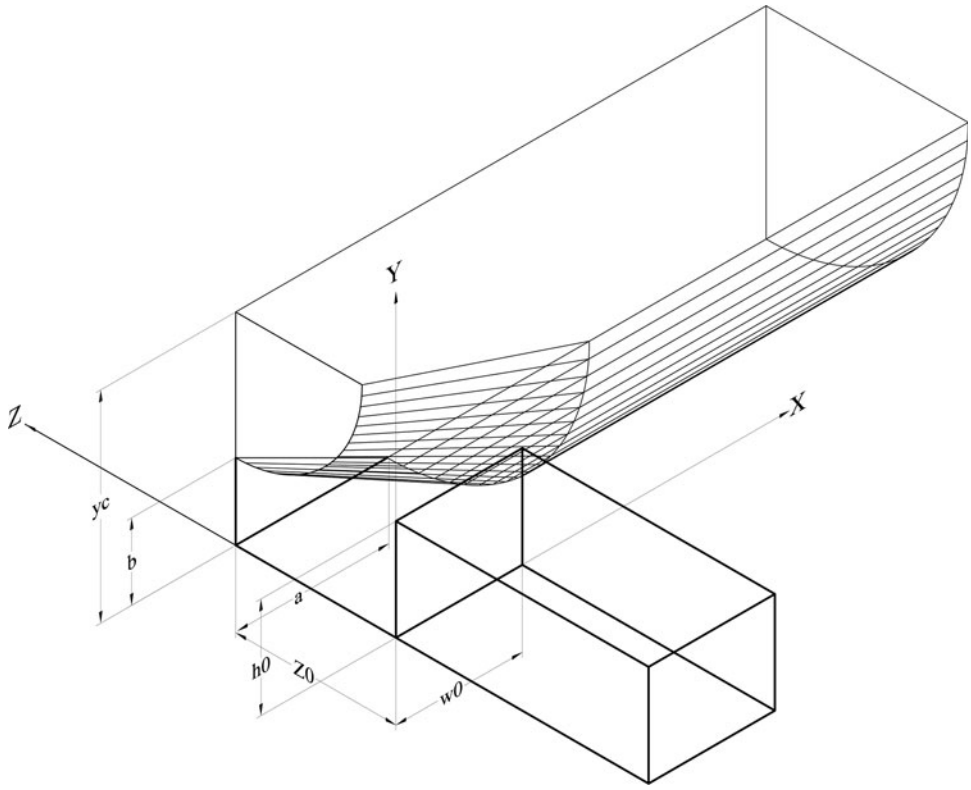

Fig. 5 A quarter of the deformation zone in a single rectangle-to-diamond pass

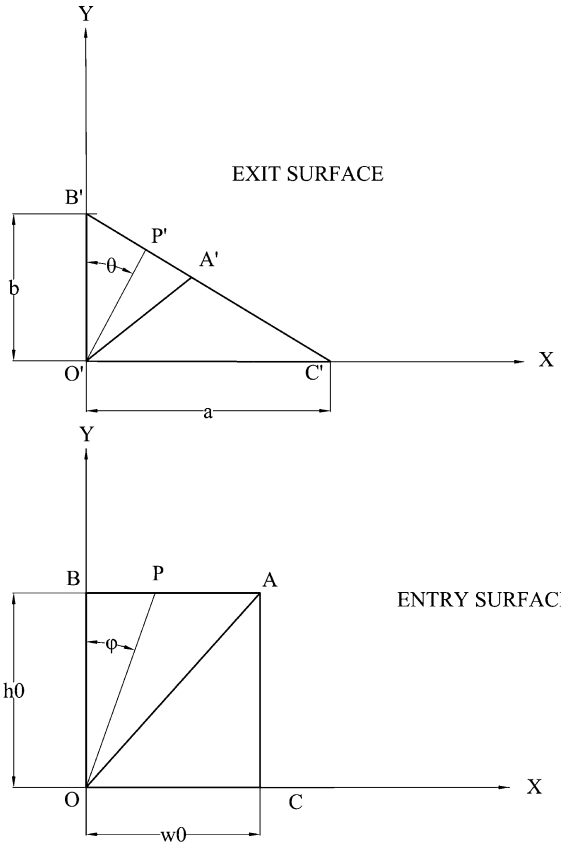

Fig. 6 Entry and exit cross sections in first half of the deformation zone in the rectangle-to-diamond pass

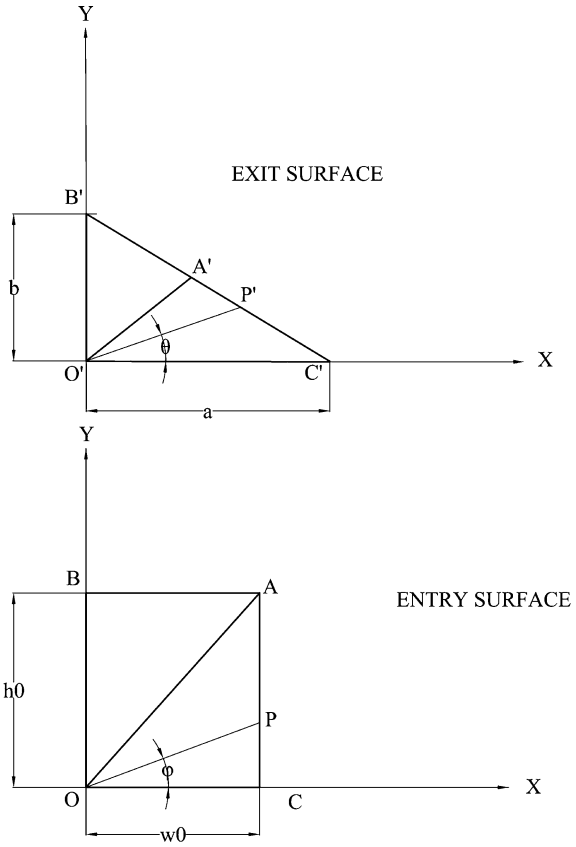

Fig. 7 Entry and exit cross sections in second half of the deformation zone in the rectangle-to-diamond pass

The velocity field in this section can be expressed as

$$M' = \frac{-\pi u V_e w_0^2}{4\cos^2\left(\frac{\pi q}{4}\right)\left[(f'_q g'_u - f'_u g'_q) - \frac{h'_q}{h'_t}(f'_t g'_u - f'_u g'_t) - \frac{h'_u}{h'_t}(f'_q g'_t - f'_t g'_q)\right]}$$

$$V'_x = \frac{f'_t}{h'_t} V'_z \qquad \text{(Eq 25)}$$

$$V'_y = \frac{g'_t}{h'_t} V'_z$$

The velocities derived satisfy both the incompressibility and the velocity continuity conditions. To ensure that velocity boundary conditions are also met, the first subsidiary constraint mentioned earlier was imposed. As the analysis involves two sections, a second condition was imposed to secure continuity of velocity at the interface of the two sections. In mathematical terms, this requires that when $q = 1$, $\vec{r}(u,q,t) = \vec{r'}(u,q,t)_{q=1}$. The relation must be true for all u and t. The rectangle-to-diamond analysis contains 13 unknown variables (including V_e) which will be determined by the optimization of the total rolling power in much the same manner as described in Section 3.1. Integration was also carried out in a similar procedure.

4. Results and Discussion

The upper bound analysis was applied to the oval-to-round and rectangle-to-diamond passes and results were compared with other methods discussed in the literature.

4.1 Oval-to-Round Pass

The oval-to-round pass was evaluated against the experiment/analysis carried out by Kennedy (Ref 3). Table 1 outlines the analytical conditions for the oval-to-round pass.

The material is low-carbon steel—AISI 1018—and rolling was performed at 1090° in which the flow stress may be described by (Ref 3)

$$\bar{\sigma} = 77.5\dot{\bar{\varepsilon}}^{0.192}\ \text{MPa} \qquad \text{(Eq 26)}$$

where $\dot{\bar{\varepsilon}}$ is the effective strain rate defined as

$$\dot{\bar{\varepsilon}} = \left(\frac{2}{3}\dot{\varepsilon}_{ij}.\dot{\varepsilon}_{ij}\right)^{\frac{1}{2}} \qquad \text{(Eq 27)}$$

Figures 8-12 illustrate various cross sections within the deformation zone, from $z/z_0 = 0$ to $z/z_0 = 1$, as predicted by the present method. In each figure, the cross-sectional shape predicted by Ref 3 has been superimposed.

Table 1 Analytical conditions for a single oval-to-round sequence

Oval-to-round pass sequence	Analytical conditions
Entry cross section dimensions	$2a$ = 23.8 mm, $2b$ = 32.9 mm
Exit cross section dimensions	R = 12.7 mm
Area reduction	17%
Roll gap	1.58 mm
Roll tangential velocity	254 mm/s

It can be observed from Fig. 8 to 12 that in all cases the present study predicts a cross section closer to the actual roll surface than Ref 3. Due to the streamline formulation, the present analysis predicts a curved, continuous upper surface while Ref 3 includes a flat upper side, remnant of a preceding square-to-oval pass.

Roll torque was calculated in various roll pass dimensions to incorporate several area reduction values $(Q = 1 - (A_{ex}/A_e))$ and by applying different frictional conditions; m = 0.2, 0.4, 0.6, 0.75. The effect of friction on roll torque was investigated in Fig. 13.

It should be noted that for a given rolling operation with specific rolling conditions, the friction shear factor is a constant, the amount of which is determined from experiments, most

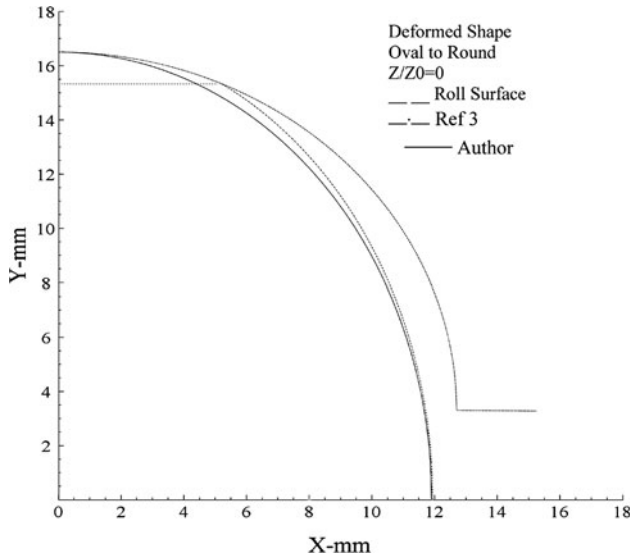

Fig. 8 Entry cross section in the oval-to-round pass as predicted by this study and Kennedy (Ref 3). The flat upper side is remnant of a previous square-to-oval pass

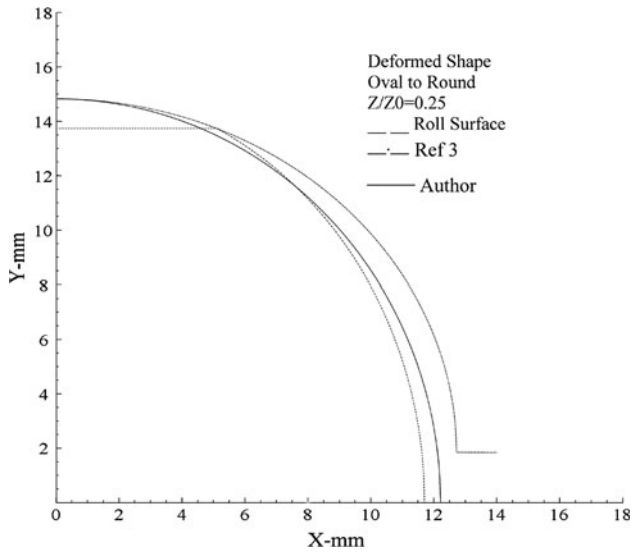

Fig. 9 Intermediate cross section at $Z/Z_0 = 0.25$ in the oval-to-round pass. Ref 3 is superimposed

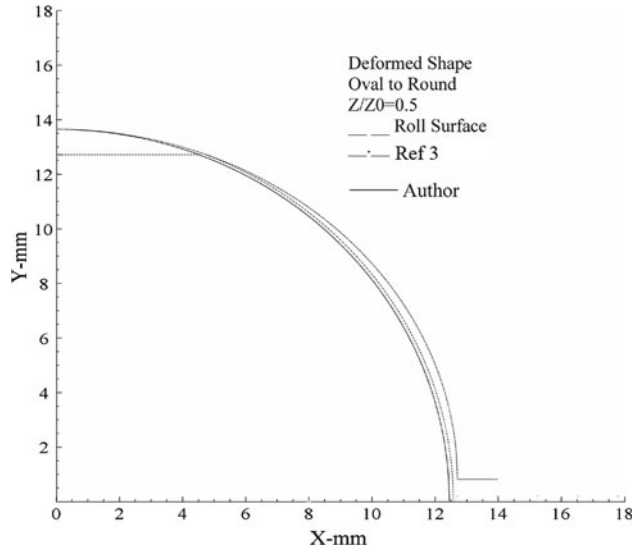

Fig. 10 Intermediate cross section at $Z/Z_0 = 0.5$ in the oval-to-round pass. Ref 3 is superimposed

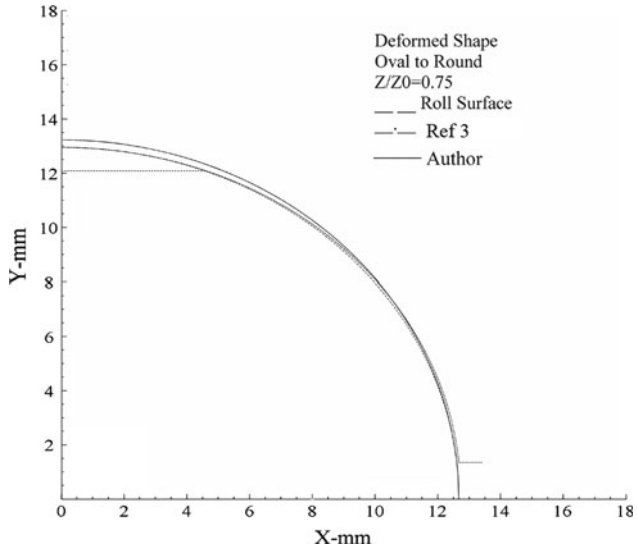

Fig. 11 Intermediate cross section at $Z/Z_0 = 0.75$ in the oval-to-round pass. Ref 3 is superimposed

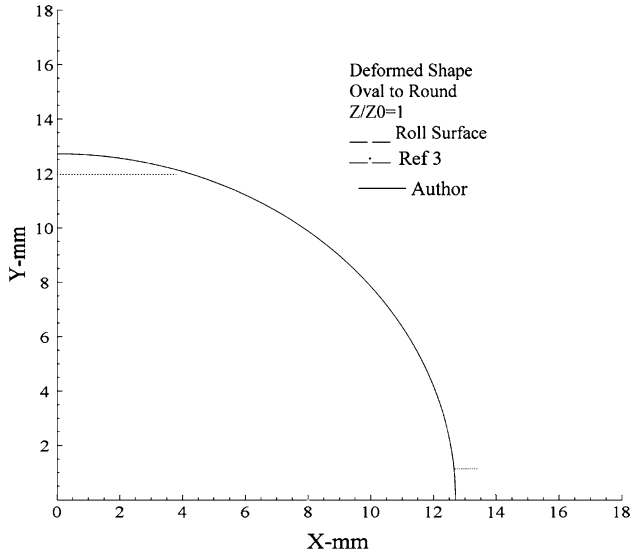

Fig. 12 Exit cross section in the oval-to-round pass as predicted by this study and Ref 3

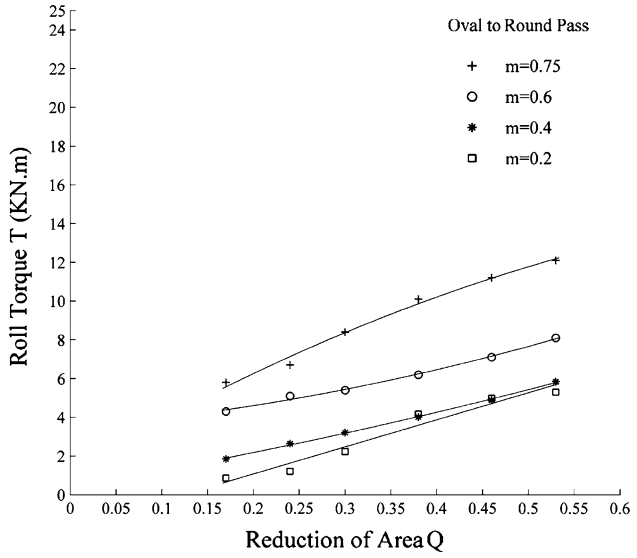

Fig. 13 The effect of friction on roll torque in various area reduction values

famously the ring test. However, for the purpose of this study, different friction shear conditions were assumed to clarify the effect of friction on rolling conditions.

The same area reduction and friction factor values were used to investigate the effect of increasing area reduction values on the average rolling pressure to flow stress ratio as shown in Fig. 14. Average rolling pressure was obtained by dividing the roll separating force by average contact area. To find the roll separating force, the slab method of analysis (Ref 3) has been used.

It can be seen from Fig. 13 and 14 that both the roll torque and the average rolling pressure to flow stress ratio increase with increasing reduction and friction factor values, in effect requiring greater rolling power. The friction factor directly affects the power required to overcome friction forces and thus the total rolling power. The effect of reduction is more subtle, influencing both entry and exit cross section dimensions, velocity fields, and all the components of power required for rolling.

The oval-to-round pass was also compared against the analytical method proposed by Bayoumi (Ref 6) and part of the experiment carried out in Ref 2. This experiment includes a four-step round-to-oval-to-round-to-oval-to-round rolling sequence, and the present analysis was used to simulate the intermediate oval-to-round sequences.

Low-carbon AISI-1080 steel was used as the rolling material, rolling temperature was assumed to be 1090 °C and flow stress was taken to be similar to 27. Table 2 outlines the dimensions for the two simulated sequences.

Table 3 shows average rolling power and exit velocity as determined by the flow-line field solution in Ref 6, experiment (Ref 2), and the upper bound method. Good conformance was

found between experimental results and the results from this study, although the present method slightly overestimates power and velocity due to the inherent tendency of the upper bound method.

The effect of increasing friction shear factor on roll torque for both simulated sequences is shown in Fig. 15 and 16, which also show the results from the flow-line field solution (Ref 6). Again, conformance was found between the two sets of results, with the same slight overestimation for the upper bound method.

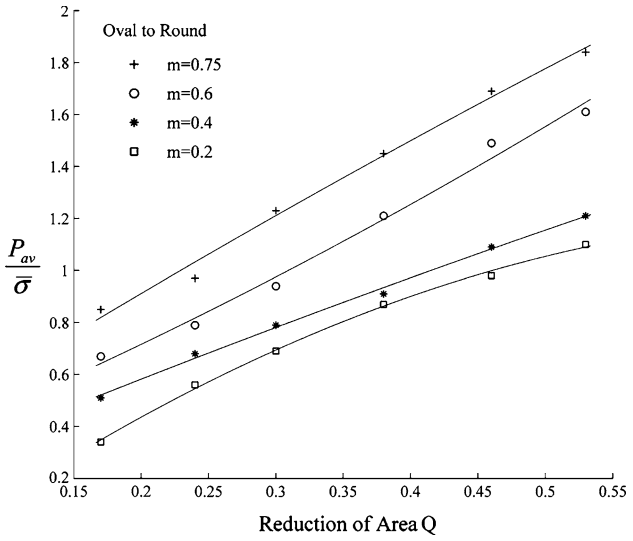

Fig. 14 The effect of friction on average rolling pressure to flow stress ratio in various area reduction values

Table 2 Rolling dimensions and conditions for the intermediate oval-to-round passes of a four-step round-to-round rolling sequence (Ref 2, 6)

Pass sequence number:	2	4
Pass geometry	Oval-to-round	Oval-to-round
Exit cross section dimensions	∅20.1 mm	∅14.2 mm
Entry cross section dimensions (major axis × minor axis)	148 × 43 mm^2	30.1 × 10.4 mm^2
Roll center distance	280 mm	280 mm
Area reduction	36.51%	35.5%
Rotational speed	105 rpm	198.5 rpm
Roll gap	2.5 mm	2 mm

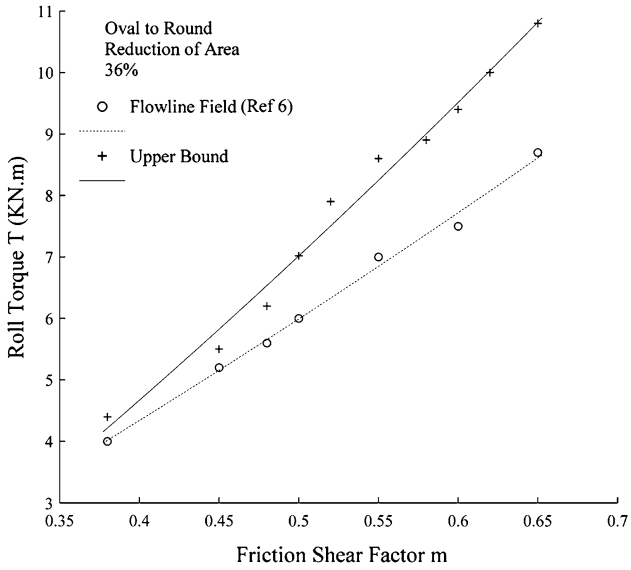

Fig. 15 The effect of increasing friction shear factor on roll torque for pass no. 2 determined from the upper bound method and the flow-line field solution (Ref 6)

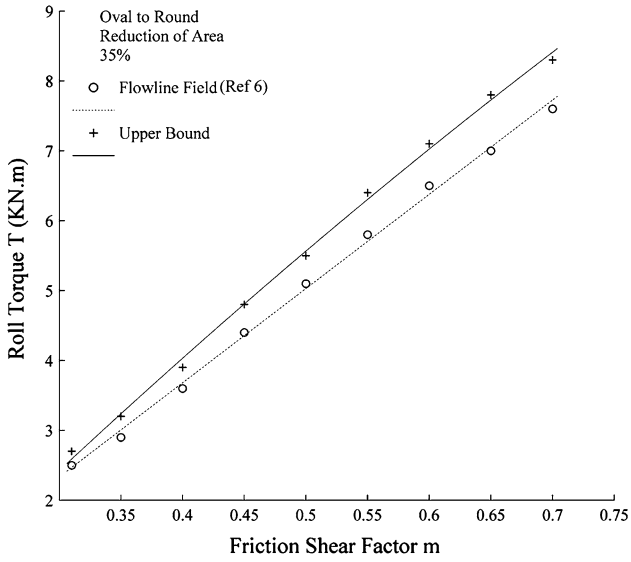

Fig. 16 The effect of increasing friction shear factor on roll torque for pass no. 4 determined from the upper bound method and the flow-line field solution (Ref 6)

Table 3 Average rolling pressure and exit velocity calculated from the present study compared to actual experiment (Ref 2) and the flow-line field solution (Ref 6)

	Pass no. 2			Pass No. 4		
	Friction factor, m	Average rolling pressure, P_{av}, MPa	Billet exit velocity, V_{ex}, m/s	Friction factor, m	Average rolling pressure, P_{av}, MPa	Billet exit velocity, V_{ex}, m/s
Experiment (Ref 2)	0.468	113.8	1.458	0.378	136.2	2.903
Upper bound method (Authors)	0.468	116.6	1.507	0. 378	141.9	3.022
Flow-line field method (Ref 6)	0.468	106	1.493	0.378	120	2.899

Table 4 Analytical conditions for the single rectangle-to-diamond pass

Rectangle-to-diamond			
Rolling temperature	**Rotational speed**	**Roll diameter**	**Incoming billet dimensions**
15 °C	20 RPM	50 mm	Length: 300 mm Thickness: 10 mm Width: 15, 20, 25 mm

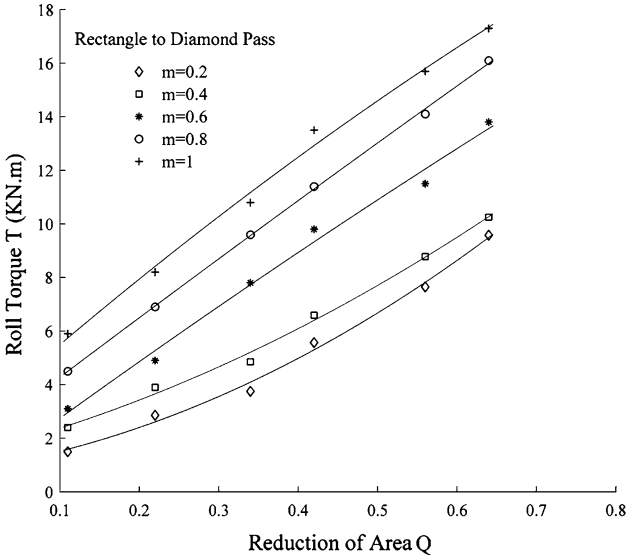

Fig. 17 The effect of friction on roll torque with various area reduction values

4.2 Rectangle-to-Diamond pass

Rectangle-to-diamond simulation was carried out under conditions extracted from an analytical solution attempted in Ref 5. The analysis assumes cold (temperature 15 °C) rolling of a Pb-0.9%wt-Sb alloy whose flow stress is expressed by (Ref 5)

$$\bar{\sigma} = 49.3\dot{\bar{\varepsilon}}^{0.04}\bar{\varepsilon}^{0.25}\ \text{MPa} \qquad \text{(Eq 27)}$$

where $\bar{\varepsilon}$ is the average value of effective strain through the deformation zone, estimated as (Ref 3):

$$\bar{\varepsilon} = \frac{1}{z_0}\int_0^{z_0}\left[\frac{2}{3}\left(\varepsilon_x^2 + \varepsilon_y^2 + \varepsilon_z^2\right)\right]^{\frac{1}{2}} \qquad \text{(Eq 28)}$$

Other analytical conditions are shown in Table 4.

The effect of increasing friction shear factor values on roll torque and roll average pressure to flow stress ratio with different area reduction values was investigated in Fig. 17 and 18.

5. Summary and Conclusions

A method has been proposed to analyze external shape, roll torque, average roll pressure, and exit velocity for the shape rolling of geometrical entities without protrusions. The method employs the upper bound solution coupled with a numerical

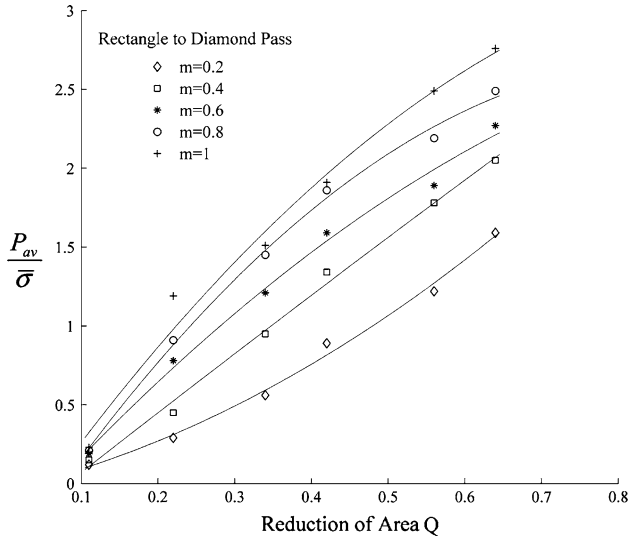

Fig. 18 The effect of friction on average rolling pressure to flow stress ratio with various area reduction values

optimization of the total power required to deform the material and in the process determines unknown variables. The upper bound method presented is based on a new application of parametric curve formulation to define streamlines within the deformation zone. Assumptions were made in order to sufficiently simplify the complex metal flow patterns in rolling to make analysis possible. Kinematically admissible velocity fields were derived from the parametric curve formulation, and an upper bound was established on rolling power required.

The authors have made the following conclusions from the comparison between the results obtained from this analysis and experimental/analytical studies by other authors:

- The shape rolling analysis presented is capable of accurately predicting external shapes in different cross sections in the deformation zone, despite its inability to incorporate cross sections that are not geometrically definable.
- The shape rolling analysis presented is capable of accurately predicting roll torque and average roll pressure. However, compared to experiments, the upper bound method somewhat overestimates torque and pressure. In actual practice, though, this is considered an advantage since these slightly higher values ensure the feasibility of the rolling operation.
- For sections in which the deforming material initiates contact with the roll groove surface toward the outer edge of the entry cross section, such as the rectangle-to-diamond pass, additional parameters are required to allow an accurate representation of the deformation zone. In contrast, passes in which contact is initiated toward the inner edges of the entry cross section, such as the oval-to-round pass, are simpler to analyze. The additional parameters entail inclusion of additional surfaces and curves, complicating the analysis and slowing convergence to optimum. The upper bound analysis is therefore less accurate than that for the sections which initiate contact toward the inner edges.
- The method presented obviates the need for complicated and, in most cases computationally overpowering, FEM simulation of the rolling passes. It also provides a basis for further expansion of the method to include other rolling passes as well as other metal forming operations.

References

1. K. Lange, Ed., *Handbook of Metal Forming*, SME Publications, Dearborn, MI, 1985
2. Z. Wusatowski, *Fundamentals of Rolling*, Pergamon Press, New York, 1969
3. K.F. Kennedy, "A Method for Metal Deformation and Stress Analysis in Rolling," PhD Thesis, Ohio State University, 1986
4. R. Hill, A General Method of Analysis for Metal Deformation Processes, *J. Mech. Phys. Solid*, 1963, **11**, p 305–326
5. Y. Saito, Y. Kusumoto, T. Hattori, and K. Kato, Deformation Analysis in Shape Rolling Using an Upper Bound Method, *Adv. Technol. Plasticity*, 1984, **11**, p 1190–1199
6. L.S. Bayoumi, Flow and Stresses in Round-Oval-Round Pass Sequence, *Int. J. Mech. Sci.*, 1998, **40**(12), p 1223–1234
7. S.I. Oh and S. Kobayashi, An Approximate Method for a Three-Dimensional Analysis of Rolling, *Int. J. Mech. Sci.*, 1975, **17**, p 293–305
8. N. Kim, S. Lee, W. Shin, and R. Shivpuri, Simulation of Square-to-Oval Single Pass Rolling Using a Computationally Effective Finite and Slab Element Method, *J. Eng. Ind. Trans. ASME*, 1992, **114**, p 329–335
9. S. Lee, W. Shin, and R. Shivpuri, Investigation of Two Square-to-Round Multipass Rolling Sequences by the Slab-Finite Element Method, *Int. J. Mach. Tool. Manuf.*, 1997, **32**(3), p 315–327
10. J.J. Park and S.I. Oh, Application of Three Dimensional Finite Element Analysis to Shape Rolling Processes, *J. Eng. Ind. Trans. ASME*, 1990, **112**, p 36–46
11. K. Mori and K. Osakada, Non-Steady-State Simulation of Three-Dimensional Deformation Around Front and Rear Ends in Shape Rolling by the Finite Element Method, *Trans. NAMRI/SME*, 1991, **19**, p 9–14
12. K. Mori and K. Osakada, FEM Simulator with Mesh Generator for Shape Rolling, *Trans. NAMRI/SME*, 1993, **21**, p 9–15
13. N. Kim, S. Kobayashi, and T. Altan, Three Dimensional Analysis and Computer Simulation of Shape Rolling by the Finite and Slab Element Method, *Int. J. Mach. Tool. Manuf.*, 1992, **31**(4), p 553–563
14. S.H. Hsiang and S.L. Lin, Application of 3D FEM-Slab Method to Shape Rolling, *Int. J. Mech. Sci.*, 2001, **43**, p 1155–1177
15. S.Y. Kim and Y.T. Im, Three Dimensional Finite Element Analysis of Non-Isothermal Shape Rolling, *J. Mater. Process. Tech.*, 2002, **127**, p 57–63
16. A.A. Milenin, H. Dyja, and S. Mróz, Simulation of Metal Forming During Multi-Pass Rolling of Shape Bars, *J. Mater. Process. Tech.*, 2004, **153–154**, p 108–114
17. F. Capece Minutolo, M. Durante, F. Lambiase, and A. Langella, Dimensional Analysis in Steel Rod Rolling for Different Types of Grooves, *J. Mater. Eng. Perform.*, 2005, **14**(3), p 373–377
18. S. Behzadipour, A. Khajepour, J.G. Lenard, and J. Biglou, A New Shape Change Quantification Method for Estimation of Power in Shape Rolling, *J. Mater. Process. Tech.*, 2004, **148**, p 353–361
19. W. Johnson and P.B. Mellor, *Engineering Plasticity*, Ellis Harwood Ltd., Chichester, UK, 1983
20. K. Abrinia, "A Generalised Upper Bound Solution for Three-Dimensional Extrusion of Shaped Sections Using Bilinear and Advanced Surface Dies," PhD Thesis, University of Manchester Institute of Science and Technology, 1990
21. D. Qiulin and B.J. Davies, *Surface Engineering Geometry for Computer-Aided Design and Manufacture*, Ellis Horwood Ltd., John Wiley & Sons, Hampstead, UK, 1987